Case Studies in Construction Materials 5 (2016) 1–18

Contents lists available at ScienceDirect

Case Studies in Construction Materials

journal homepage: www.elsevier.com/locate/cscm

Case study

Applications of smart piezoelectric materials in a wireless admittance monitoring system (WiAMS) to Structures—Tests in RC elements

Constantin E. Chalioris[a,*], Chris G. Karayannis[a], Georgia M. Angeli[a], Nikos A. Papadopoulos[a], Maria J. Favvata[a], Costas P. Providakis[b]

[a] Department of Civil Engineering, Democritus University of Thrace, Xanthi 67100, Greece
[b] School of Architectural Engineering, Technical University of Crete, Chania 73100, Greece

ARTICLE INFO

Article history:
Received 11 January 2016
Received in revised form 23 March 2016
Accepted 25 March 2016
Available online 28 April 2016

Keywords:
Reinforced concrete (RC)
Structural health monitoring (SHM)
Flexural tests
Shear
Piezoelectric lead zirconate titanate (PZT)
Damage assessment

ABSTRACT

The application of an innovative real-time structural health monitoring system is studied through tests performed on flexural and shear-critical reinforced concrete elements subjected to monotonic and cyclic loading. The test set-up involves a Wireless impedance/Admittance Monitoring System (WiAMS) that comprises specially manufactured small-sized portable devices to collect the voltage frequency responses of an array of smart piezoelectric transducers mounted on structural members of reinforced concrete constructions. Damage detection and evaluation is achieved using the in-situ measurements of the integrated piezoelectric sensors/actuators signals at the healthy state of the member and at various levels of damage during testing. Three different installations of Piezoelectric lead Zirconate Titanate (PZT) transducers are examined: (a) epoxy bonded PZTs on the surface of the steel reinforcing bars of the flexural elements, (b) PZTs embedded inside the concrete mass of the shear-critical beams and (c) externally epoxy bonded PZTs attached to the concrete surface of the tested elements. The smart piezoelectric materials have been pre-installed before testing based on the potential flexural and shear cracking of the elements. Quantitative assessment of the examined damage levels using values for the statistical damage index is also presented and discussed. Voltage signals and index values acquired from the PZTs' measurements using the proposed wireless monitoring technique demonstrated obvious discrepancies between the frequency response of the healthy and the examined damage levels for every tested element. These differences clearly indicate the presence of damage, whereas their gradation reveals the magnitude of the occurred damage. Promising results concerning the prediction of the forthcoming fatal failures at early damage stages have also been derived.

1. Introduction

Materials aging of Reinforced Concrete (RC) structures, earthquake excitations, corrosion of steel reinforcement and fire exposure have been the cause of serious structural damage and of high costs in repair and maintenance. Concrete

* Corresponding author.
E-mail address: chaliori@civil.duth.gr (C.E. Chalioris).

http://dx.doi.org/10.1016/j.cscm.2016.03.003

deterioration and damage in critical RC members adversely impact the ability of structures to withstand future operating conditions and increase risk to fatal failures and catastrophic collapses if not controlled. Recently developments of various non-destructive and Structural Health Monitoring (SHM) techniques have been made with respect to real-time surveillance, continuous inspection and in-situ testing techniques to help ensure continuous safe, functional and economical operation of RC structures. Even more, SHM is becoming extremely important in RC structures that withstand critical shear mechanisms which lead to fragile and abrupt failure modes. Even minor incipient shear damage in deficient shear-critical RC elements, such as beam-column joints, short columns and deep beams, could be the cause of catastrophic collapse [3,10,32,35,42].

The implementation of smart materials such as Piezoelectric lead Zirconate Titanate (PZT) in SHM techniques is a rather recent development with promising results. It has emerged due to the advantageous characteristics of these materials combined with the merits of the Electro-Mechanical Impedance (EMI) or its reverse admittance method that uses electro-mechanical signals extracted from PZT transducers mounted on RC members as damage indicators [33,36,39,46,48].

A PZT transducer produces electrical charges when subjected to a strain field and conversely it produces mechanical strain when an electrical field is applied. The impedance-based SHM approach utilizes the electro-mechanical properties of these smart materials that are related with the mechanical impedance of the host structural members, which is affected by the presence of any structural damage. In this way, the impedance extracts and its inverse, the admittance, constitute the properties on which the PZT approach is based for the SHM of RC structures. The produced effects by the structural damage on the PZT electrical signals are vertical enlargement or/and lateral shifting of the baseline signals of the initially healthy structure [9,18,49]. Numerical studies that simulate electro-mechanical admittance monitoring procedures utilizing PZTs to detect and localize cracking in concrete beams have also been presented [15,24,28,43]. In addition, identification of damage due to the corrosion of steel reinforcing bars and debonding between bars and concrete have been investigated experimentally and analytically using bonded PZT transducers on the surface of the steel bars [16,29,30,40,41]. Furthermore, real-time monitoring of concrete compressive strength gain using bonded PZT patches showed promising results [25,26,28,34,45].

Failures in shear-deficient RC elements are associated with brittle catastrophic collapses. When principal tensile stresses exceed the tensile strength of concrete, diagonal cracking occurs in the shear span and the behaviour of a concrete element under shear stresses is mainly characterised by the tensile strength of the material [4,19,31]. It has been found that the ratio of the transverse shear reinforcement, the ratio of the tensional reinforcement and the span-to-depth ratio control the inclination of the shear diagonal cracking of shear-critical RC beams [14]. It is also known that the ultimate shear strength of RC beams is calculated by a superposition of the shear strength of beams without web reinforcement and the strength provided by the shear reinforcement [7,8]. However, the formation of critical shear diagonal cracking of RC beams without web reinforcement is crucial for the determination of the onset of diagonal cracking of common RC beams with bars and stirrups. Consequently, any improvement of the existing SHM techniques to detect in real-time the first appeared diagonal cracks in a RC beam and to assess their severity before the inevitable brittle shear failure of the element is essential. A first approach to diagnose damage at early cracking stages of shear-critical RC beams using the admittance measurements of embedded and surface attached PZTs through a non-portable EMI monitoring system has recently been attempted by Chalioris et al. [5] and Voutetaki et al. [44].

Piezoelectric materials embedded inside the concrete mass as “smart aggregate” and external piezoelectric patches bonded on the concrete surface have been used to monitor concrete structural elements. It has been found so far that the surface bonded PZTs are not sufficiently effective for monitoring a large area or the entire concrete structure due to their small sensing range. On the other hand, the embedded smart piezoelectric aggregates can be employed to monitor large areas with a reasonably low actuation signal [5,11,17,22,37,38].

It is noted that most of the developed SHM systems using the EMI technique and PZT transducers are until now not portable and therefore they have obvious difficulties and limitations to be applied in-situ on existing structures. There are only a few portable and wireless EMI monitoring systems that use smart piezoelectric materials in RC elements [12,20,23]. Preliminary tests of the innovative, wireless, portable, lightweight, real-time impedance monitoring sensing system that is experimentally investigated herein have been reported in the recent works of Providakis and Liarakos [25,27], Providakis et al. [26], Chalioris et al. [6] and Voutetaki et al. [44].

In this work the effectiveness of the developed Wireless impedance/Admittance Monitoring System (WiAMS) to diagnose damage is tested in a series of two flexural RC beams under monotonic loading, a flexural RC element under cyclic loading and a shear-critical RC beam under monotonic loading. Quantitative assessment of the examined damage levels in all tested RC elements using values for the statistical damage index is also attempted. This study also aims to evaluate the performance of this new SHM system in different RC elements for real-time surveillance, continuous inspection and in-situ testing for the prediction of the forthcoming final failure at early damage stages.

2. Structural health monitoring and damage evaluation technique

2.1. Electro-mechanical impedance (EMI) method

The Electro-Mechanical Impedance (EMI) technique uses Piezoelectric lead Zirconate Titanate (PZT) transducers exhibiting their characteristic feature to generate surface electric charge in response to an applied mechanical stress and undergo mechanical deformation in response to an applied electric field. Thus, when a PZT that is mounted on a structure is

actuated, a potential damage induces change in the mechanical impedance (or its reverse admittance) of the structure and this change reflects on the electrical signal of the PZT. When a structure is regularly monitored by extracting the signal to the exciting frequency of the installed PZTs, the changes in their signatures become indicative of the presence of structural damage [21,24]. In this way, any structural damage in the monitored RC element such as concrete cracking or steel yielding could be detected through the changes of the signatures of the mounted piezoelectric transducers.

In the adopted structural health monitoring methodology for the detection of a potential damage in RC elements, the PZT transducers are excited for a specific frequency range and their corresponding signals are recorded simultaneously. These measurements are carried out initially on the undamaged RC element (healthy initial status) in order to record the healthy condition and to be used as a reference signature. Afterwards, the same measurements are carried out on the damaged RC element at different levels of damage. An excitation frequency range of 10 kHz to 260 kHz per step of 10 kHz by using one cycle per 10 kHz has been implemented and a harmonic excitation voltage of 10 V was amplified to the PZT transducers in the time domain range at every central frequency, as described by the expression [28–30]:

$$V_{PZT}(t) = 10\sin(2\pi\omega t) \tag{1}$$

where: V_{PZT} is the excitation voltage of the PZT, ω is the angular frequency of the driving voltage and t is the time domain range.

The interaction between PZT and the RC element is captured in the form of an admittance signature consisting of the conductance (real part) and the susceptance (imaginary part). As a result of these interactions, structural characteristics are reflected in the signature. The one-dimensional vibrations of the PZT patch are governed by the differential equation derived by Liang et al. [18] based on dynamic equilibrium of the PZT transducer. Bhalla and Soh [1] extended this approach to two dimensional structures by introducing the concept of effective impedance, deriving the following expression for complex admittance, Y, of the mounted PZT patch:

$$\overline{Y} = \frac{\bar{I}}{\overline{V}} = G + Bj = 4\omega j\frac{L^2}{h}\left[\bar{\varepsilon}_{33}^{T} - \frac{2d_{31}^2\overline{Y}^{E}}{(1-\nu)} + \frac{2d_{31}^2\overline{Y}^{E}}{(1-\nu)}\left(\frac{Z_{a,eff}}{Z_{s,eff}+Z_{a,eff}}\right)\left(\frac{\tan(kL)}{kL}\right)\right] \tag{2}$$

where: $\overline{V}$ is the harmonic alternating voltage supplied to the circuit, $\bar{I}$ is the current passing through PZT, G is the conductance (the real part of admittance), B is the susceptance (the imaginary part of admittance), j is the imaginary unit, ω is the angular frequency, L is the half-length of the patch, h is the thickness of the patch, d_{31} is the piezoelectric strain coefficient of the PZT, $Z_{a,eff}$ is the short-circuited effective mechanical impedance, $Z_{s,eff}$ is the effective structural impedance, ν is Poisson's ratio, k is the wave number related to the angular frequency, $\overline{Y}^{E}$ is the complex Young's modulus of elasticity under constant electric field and $\bar{\varepsilon}_{33}^{T}$ is the complex electric permittivity of PZT patch along axis "3" at constant stress. Any damage to the RC beam that changes its mass and stiffness characteristics will cause the structural parameters to change and will thus alter the effective structural impedance, which in turn changes the admittance Y, as defined by Eq. (2), thus serving as an indicator of the state of health of the element [40].

The absolute value of the admittance is calculated by the following equation:

$$|Y(\omega)| = \sqrt{G^2(\omega) + B^2(\omega)} \tag{3}$$

where: G is the real part (conductance) and B is the imaginary part (susceptance) of the admittance Y.

2.2. The developed wireless impedance/Admittance monitoring system (WiAMS)

The developed SHM system is initially based on the Electro-Mechanical Impedance (EMI) methodology (or its reverse electro-mechanical admittance) and utilizes the measurements of Piezoelectric lead Zirconate Titanate (PZT) transducers mounted on the structural RC element which operate as actuators and sensors simultaneously. WiAMS is the acronym for Wireless impedance/Admittance Monitoring System that estimates the impedance magnitude of a PZT transducer that is utilized in order to monitor in situ and in real-time the structural integrity of RC elements and structures. In this way, a WiAMS device sends out the interrogating waves through a PZT and receives the reflected waves at the same time. It offers extensive features such as remote control, high processing power, wireless data upload to SQL database, email notifications, scheduled, iterative impedance magnitude estimations within a frequency span from 5 kHz to 300 kHz with 1 Hz resolution. The WiAMS device consists of the following multiple custom-made modules, as shown in Fig. 1:

1. A single board computer (SBC) Raspberry Pi.
2. A custom board with the AD7357 ADC
3. A custom board with the AD9837 frequency generator
4. A custom interface board responsible for the power supply and the connection to the rest modules between them and with the Raspberry Pi.
5. The PZT driver module.

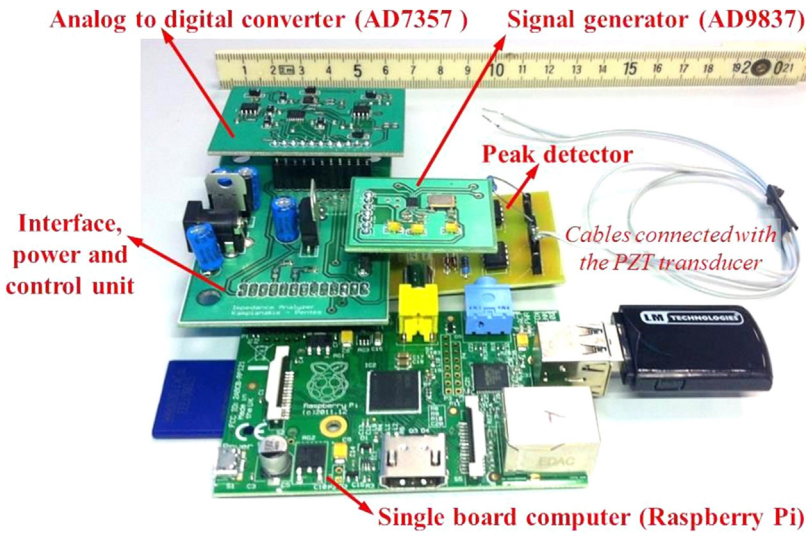

Fig. 1. The portable Wireless impedance/admittance monitoring system (WiAMS) modulus.

The impedance magnitude of the PZT is estimated by WiAMS based on the following consideration. First, the input sinusoidal voltage signal can be expressed as a function of time in the form:

$$V_{PZT}(t) = V_p \sin(\omega t) \tag{4}$$

where, $V_{PZT}(t)$ is the voltage across the direction of the axis of the width of the PZT at time t, V_p is the peak voltage of the voltage signal and ω is the radial frequency. The relationship between the radial frequency ω (in radians/second) and the frequency f (Hz) is $\omega = 2\pi f$.

In a linear system the response current signal I(t) is shifted in phase ϕ and has a different peak current I_p:

$$I(t) = I_p \sin(\omega t + \varphi) \tag{5}$$

Taking into account that every PZT transducer under a pure and high frequency sinusoidal voltage signal behaves almost like a capacitive system that tends to preserve negligible phase difference between voltage and current output signal, the impedance magnitude of the PZT at radial frequency $|Z(\omega)|$ can be evaluated by the expression:

$$|Z(\omega)| = \frac{1}{|Y(\omega)|} = \frac{V_p(\omega)}{I_p(\omega)} \cong \frac{V_p(\omega)}{\frac{V_{in}(\omega)}{|Z(\omega)|+R_f}} \tag{6}$$

where, V_{in} is the voltage output of the frequency generator and R_f is a resistor connected in series with the PZT of a circuit that consists of an efficient and simple method to measure impedance magnitude by exciting the device under test with a sinusoidal signal and measuring the amplitude of the voltage of the device.

Solving Eq. (6) in terms of $V_p(\omega)$ the peak value of the voltage across the PZT transducer can be estimated by:

$$V_p(\omega) \cong \frac{|Z(\omega)|}{|Z(\omega)| + R_f} V_{in}(\omega) \tag{7}$$

Based on the above equation, it is obvious that the voltage across the PZT transducer and especially the peak voltage signal $V_p(\omega)$ provides a solid indication of the value of $|Z(\omega)|$ being directly dependent on any observed impedance amplitude variations. In this way, under steady state conditions, if the structural integrity condition of the host structure changes then the peak amplitude of the voltage signal across the PZT transducer also changes. The application of expression (7) enables the implementation of simple and low-cost monitoring topologies compared to the traditional and complex impedance analysers.

3. Experimental program

3.1. Characteristics of the RC elements

The test program included four large-scale RC elements; two of them were subjected to flexural monotonic loading (beams FL10 M and FL12 M), one to cyclic quasi-static flexural loading (element FL12C) and one shear-critical beam to monotonic load (beam SH14 M). Following this approach, the effectiveness of the developed portable wireless monitoring

system (WiAMS) to evaluate the flexural or/and shear damage caused on RC elements during typical monotonic and cyclic tests and at various levels of loading and corresponding damage is experimentally investigated.

Geometrical and reinforcement characteristics of the RC elements are illustrated in Fig. 2. The mean concrete cylinder compressive strength was f_{cm} = 28.2 MPa. The total length of the three flexural elements was 2.7 m, the shear span was 1.0 m, the height to the width ratio was 250/200 mm and the span-to-depth ratio was 5 (see also Fig. 2a). Common closed mild steel stirrups with a diameter of 6 mm and spacing of 200 mm (Ø6/200 mm) comprised the adequate transverse reinforcement of the flexural RC elements that prevents shear failure. The bottom tensional longitudinal reinforcement of the RC beams FL10 M and FL12 M comprised two steel bars of diameter 10 mm (2Ø10) and two steel bars of diameter 12 mm (2Ø12),

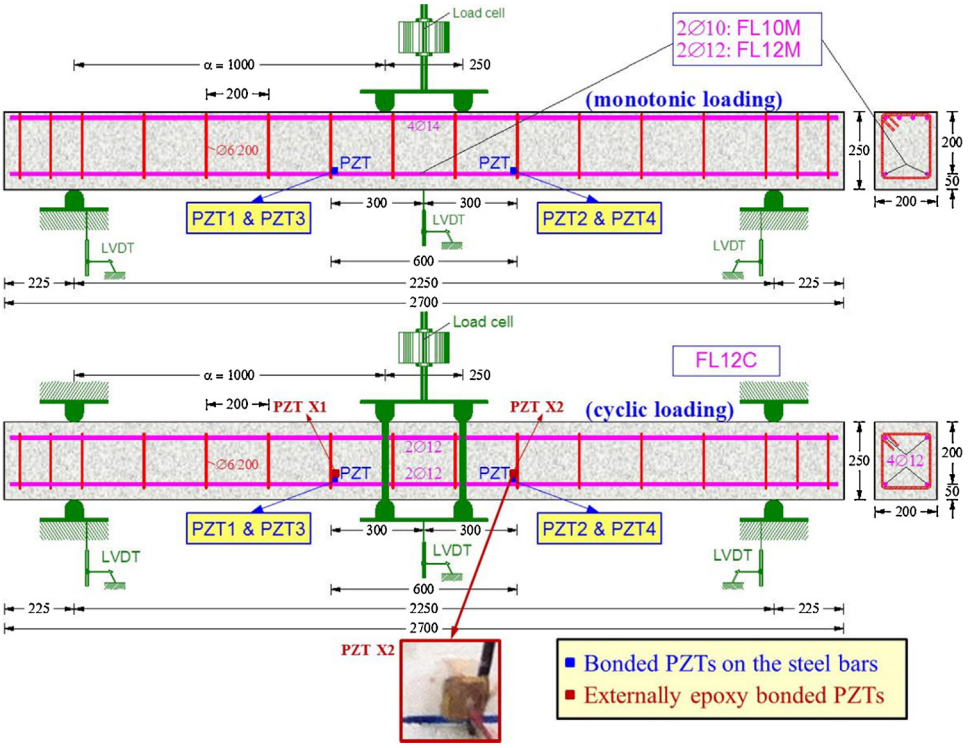

(a) Flexural elements (FL10M, FL12M and FL12C)

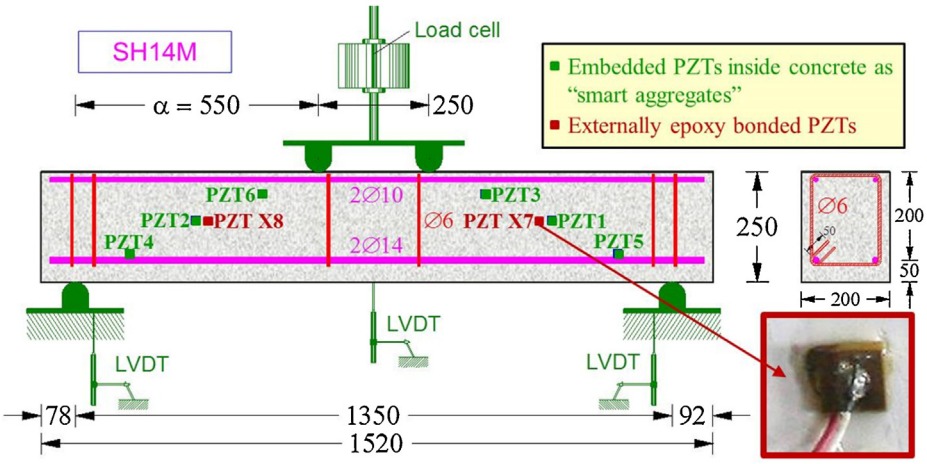

(b) Shear-critical beam (SH14M)

Fig. 2. Geometrical and reinforcement characteristics of the tested RC elements.

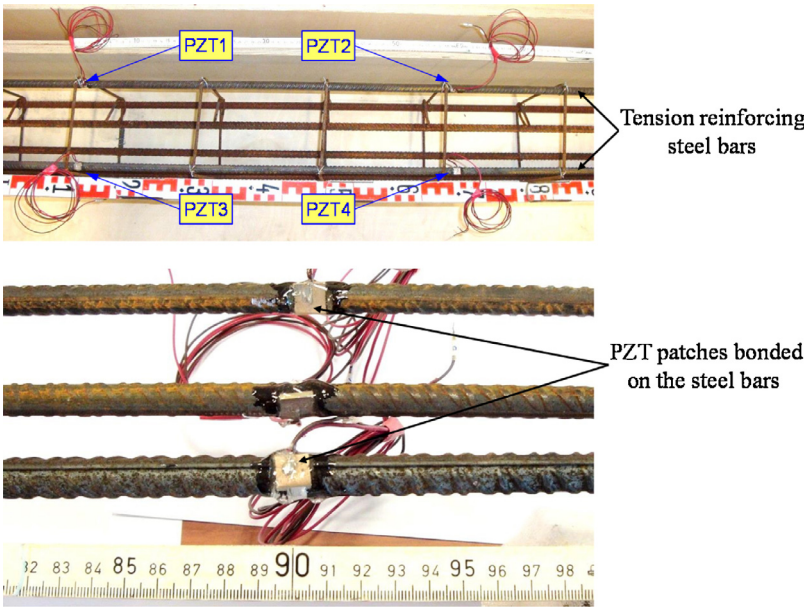

Fig. 3. Bonded PZT transducers on the tension reinforcing steel bars of the flexural RC elements before concrete casting.

respectively, whereas the amount of top compression reinforcement of both beams is high (4Ø14) in order to prevent brittle failure of the compression zone. Flexural element FL12C was symmetrically reinforced with four steel longitudinal bars of diameter 12 mm; 2Ø12 up and 2Ø12 bottom. The measured yield tensile strength values of the tensional steel bars Ø10 and Ø12 were 535 and 550 MPa, respectively.

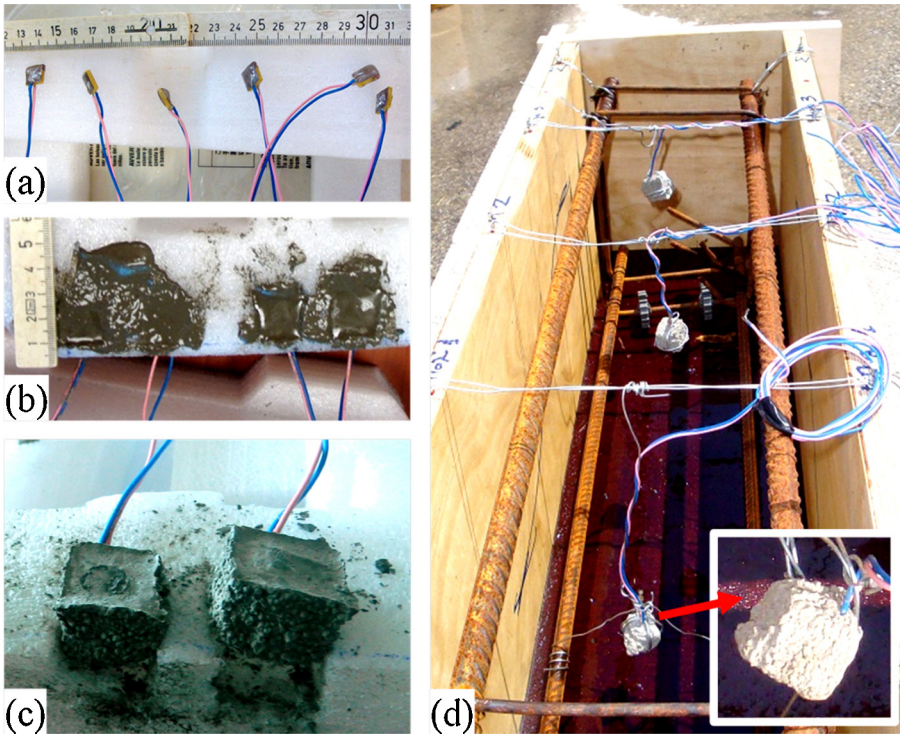

Fig. 4. Preparation steps and installation of the PZT transducers as "smart aggregates" in the shear-critical RC beam (SH14 M): (a) cables are first soldered to PZTs and then waterproofing is achieved using epoxy adhesive, (b) cement paste is poured in small foam moulds enclosing the waterproofed PZTs, (c) irregular cement cubes with embedded PZTs ("smart aggregates") are formed after demoulding the hardened cement paste and (d) installation of the "smart aggregates" inside the wooden mould of the RC beam after the placement of steel reinforcement and before concrete casting.

The total length of the shear-critical RC beam SH14 M was 1.52 m, the shear span was 0.55 m, the height to the width ratio was also 250/200 mm and the span-to-depth ratio was 2.75 (see also Fig. 2b). The bottom tensional longitudinal reinforcement of the beam comprised two steel bars of diameter 14 mm (2Ø14) and the top compression reinforcement was two bars of diameter 10 mm (2Ø10). Only a few closed stirrups of diameter 6 mm have been used to hold reinforcing bars in place. Both shear spans of the beam had no transverse web reinforcement in order to control a typical shear failure (design of a shear-critical RC beam).

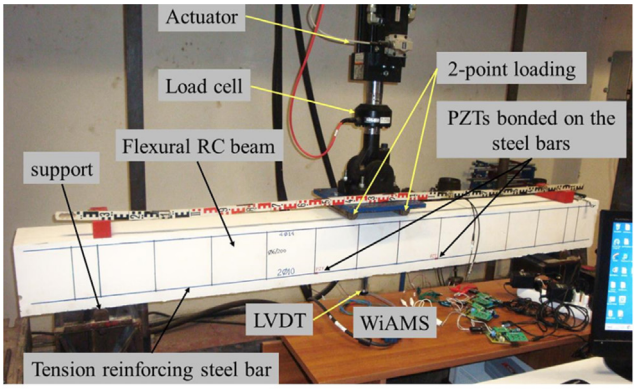

(a) Flexural beams under monotonic loading (FL10M and FL12M)

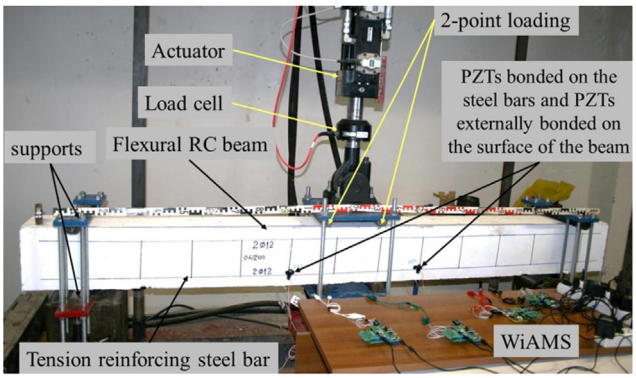

(b) Flexural element under cyclic loading (FL12C)

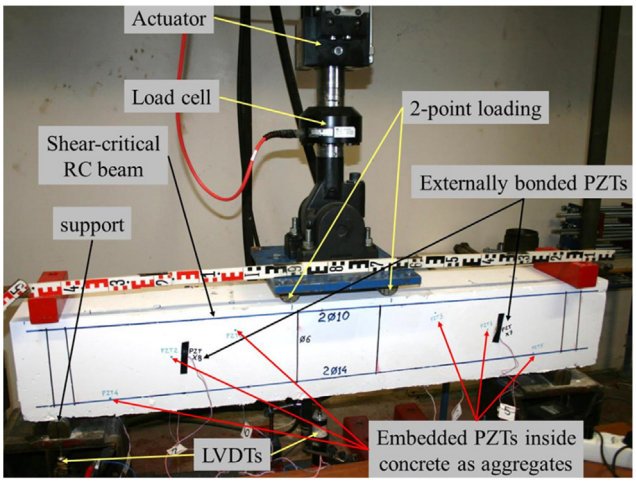

(c) Shear-critical beam under monotonic loading (SH14M)

Fig. 5. Test rigs and instrumentation.

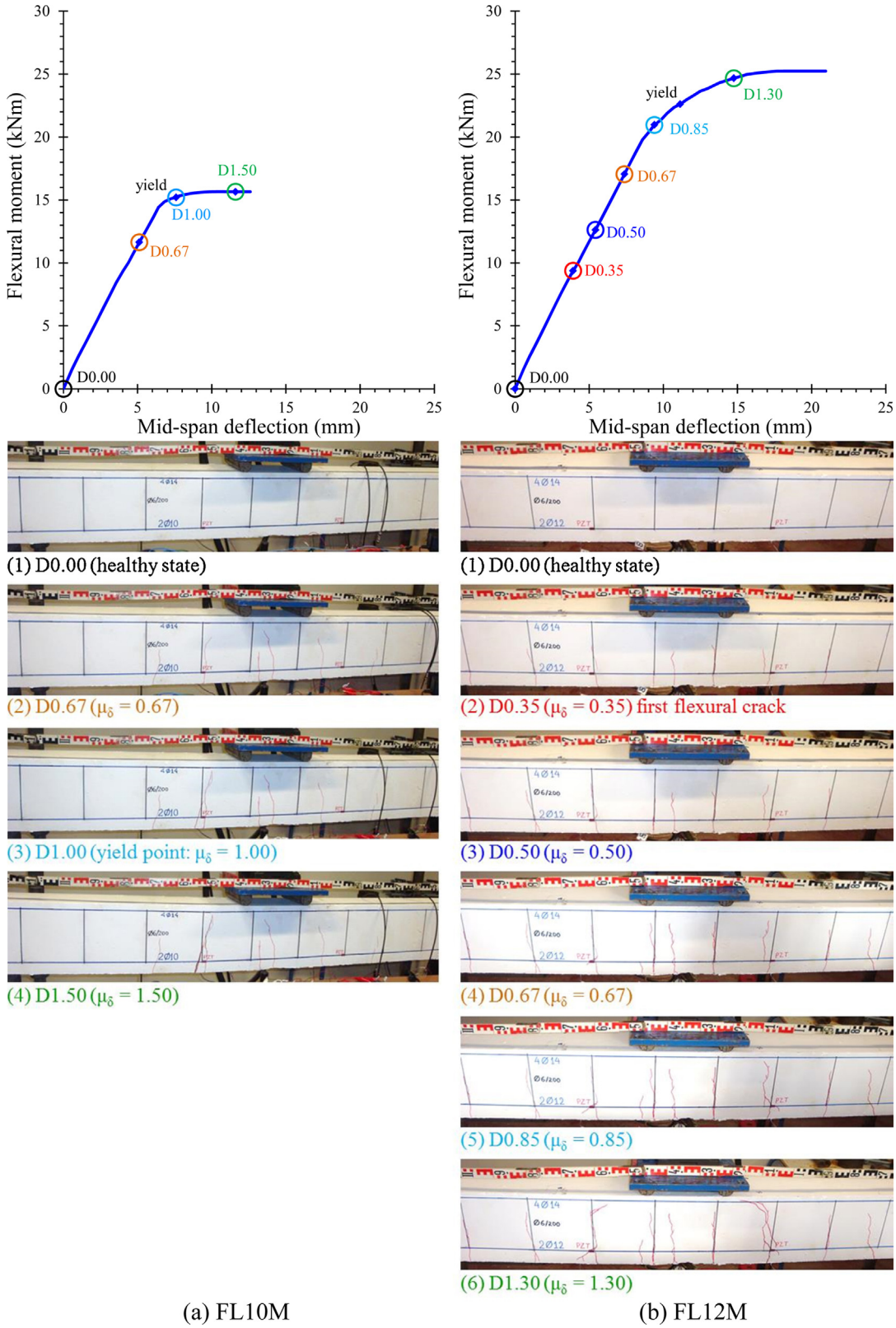

Fig. 6. Experimental behaviour and cracking patterns of the flexural RC beams under monotonic loading.

3.2. Installation of PZT transducers

Thin and small-sized PZT transducers with dimensions 10 mm × 10 mm and material mark designation PIC 255 were used. The PZT patches have been mounted on the tested RC elements as:

(a) epoxy bonded PZTs on the surface of each steel tensional reinforcing bar after a proper flattening of the bar of the flexural elements FL10 M, FL12 M and FL12C inside the concrete mass (internal PZTs),
(b) PZTs embedded inside the concrete mass of the shear-critical beam SH14 M as "smart aggregates" (internal PZTs) and
(c) externally epoxy bonded PZTs attached to the concrete surface of the specimens FL12C and SH14 M (external PZTs).

Epoxy adhesive with a high shear modulus and small thickness has been used to bond the PZTs. Two PZT patches have been bonded on the surface of each tensional steel bar of the flexural elements, as shown in Fig. 3, denoted as "PZT1", "PZT2", "PZT3" and "PZT4". A waterproof layer of the epoxy adhesive has also been applied meticulously on the top of each PZT in order to protect the patches during concrete casting and to avoid noise in their signature. Each epoxy bonded PZT on the surface of the steel bar was inside concrete and located at a distance of 300 mm from the middle of the flexural RC elements and at a distance of 600 mm from each other (see also Fig. 2a).

Concerning the embedded PZT transducers as "smart aggregates", their preparation includes the following steps, as presented in Fig. 4: Two cables were first soldered to each side of the PZT and epoxy adhesive was used to coat and to waterproof the patches (Fig. 4a). Thereafter, cement paste was poured in small foam moulds enclosing the waterproofed PZT patches (Fig. 4b). Within a few days after demoulding the hardened cement paste, irregular cement cubes with the enclosed PZTs were formed as "smart aggregates" (Fig. 4c). The PZT "smart aggregates" have been fixed inside the wooden mould of the RC beams, after the placement of the steel reinforcing bars and stirrups, but just before concrete casting (Fig. 4d). Six "smart aggregates" were embedded inside the concrete mass of the shear-critical beam SH14 M. "PZT1", "PZT3" and "PZT5" were located on the right shear span and "PZT2", "PZT4" and "PZT6" on the left shear span, across to the potential future diagonal cracks, as shown in Fig. 2b.

Furthermore, after concrete casting and demoulding the hardened concrete of the RC elements, four PZT patches with two soldered cables were carefully epoxy bonded externally on the concrete surface of the flexural element FL12C (denoted as "PZT X1" and "PZT X2") and of the shear-critical beam SH14 M (denoted as "PZT X7" and "PZT X8") as shown in Figs. 2a and b, respectively.

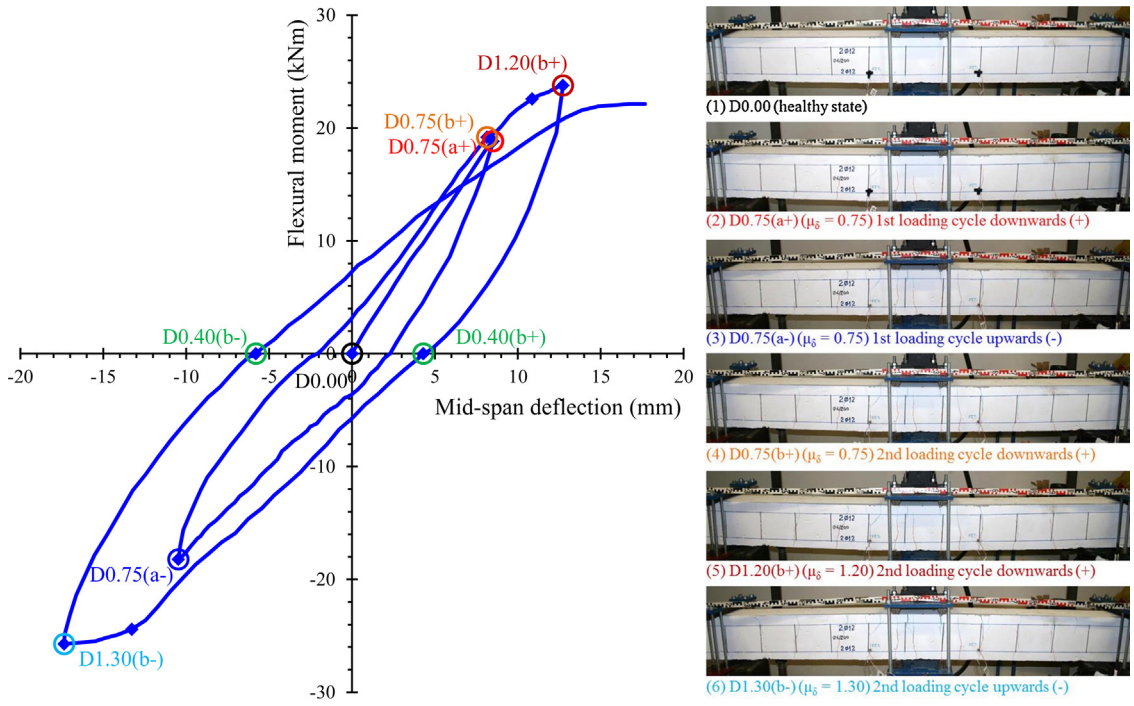

Fig. 7. Experimental behaviour and cracking patterns of the flexural RC element under cyclic loading (FL12C).

3.3. Test setup and instrumentation

A typical four-point bending scheme and setup as shown in Figs. 5a and b was adopted for the flexural monotonic testing of RC beams FL10 M and FL12 M and for the cyclic test of RC element FL12CM, respectively. Test setup and instrumentation of the shear-critical RC beam is also displayed in Fig. 5c. These test beams were supported on a rigid laboratory frame using roller supports. The imposed loading was applied at two points 250 mm apart from each other in the mid-span of each element using a steel spreader beam. The imposed load was gradually increased with a low rate using a pinned-end actuator and was measured by a load cell with accuracy equal to 0.05 kN. The net mid-span deflections of the tested elements were recorded by three Linear Variable Differential Transducers (LVDTs) with 0.01 mm accuracy. One of them was placed at the middle of the beam span and the other two at the supports (Fig. 2). Measurements for load and deflection were read and recorded continuously during the tests. In addition, voltage signatures of all the PZT transducers were recorded at different levels of the applied loading using the WiAMs experimental setup as shown in Fig. 1. A harmonic excitation voltage of 10 V is amplified to the mounted PZTs in the time domain range at every central frequency, as described by Eq. (1).

3.4. Test results and discussion

The flexural beams under monotonic loading (FL10 M and FL12 M) and the flexural element under cyclic loading (FL12C) exhibited typical flexural response, as was designed for and as expected. First flexural cracks formed at mid-span (pure bending

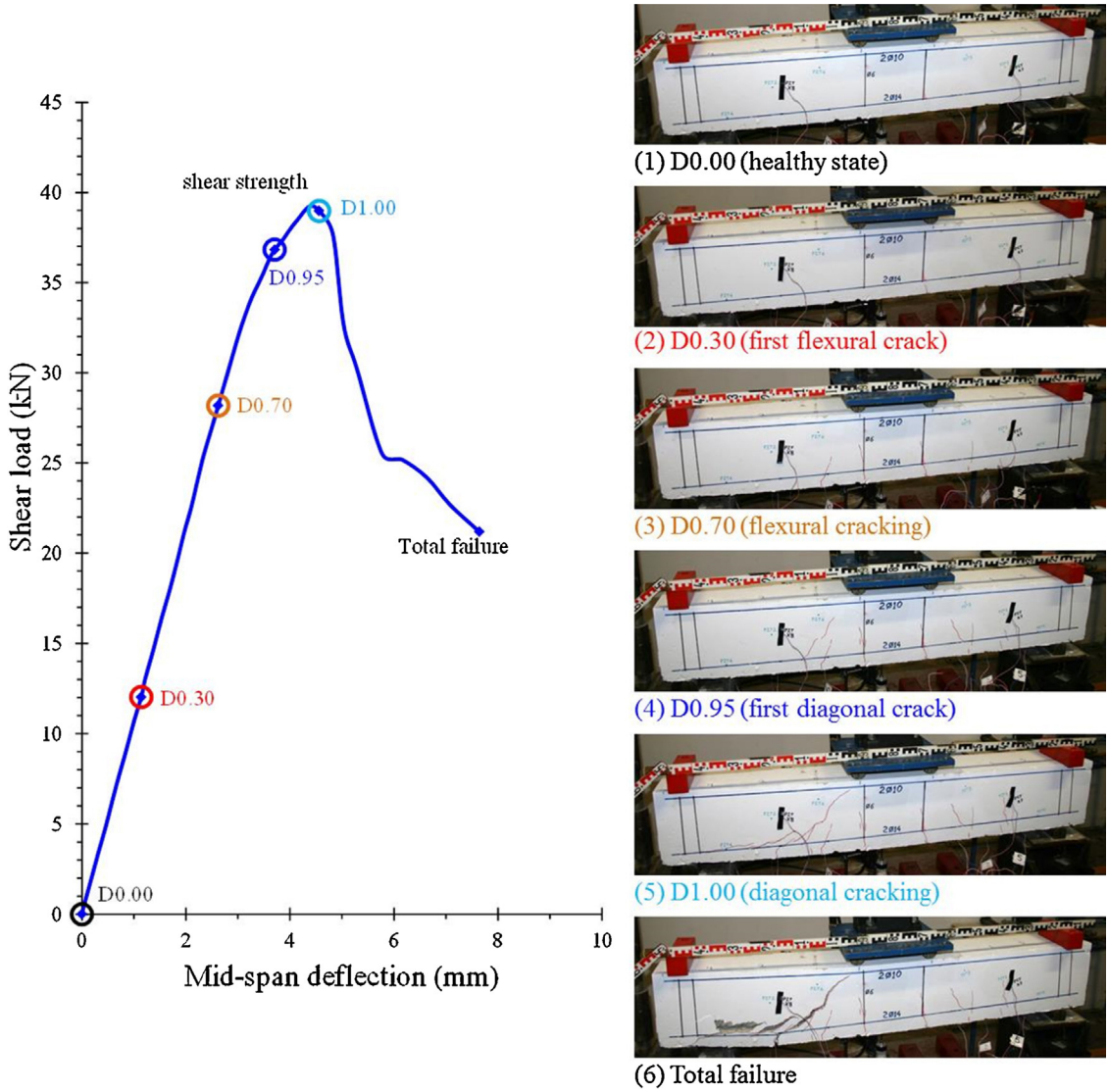

Fig. 8. Experimental behaviour and cracking patterns of the shear-critical RC beam (SH14M).

region) and perpendicular to the longitudinal axis of the beams. The increase of the applied bending moment caused flexural cracks area to spread and inevitably tensional longitudinal bars to yield. The monotonic behaviour of beams FL10 M and FL12 M is presented in Figs. 6a and b, respectively, in terms of experimental curve of flexural moment versus mid-span deflection. The cracking patterns and damage of the RC beams at different levels of loading and deformation ductility are also displayed in the photographs of Figs. 6a and b. The cyclic response of element FL12C in terms of flexural moment versus mid-span deflection curve and its cracking patterns at different levels of loading and deformation ductility are also presented in Fig. 7.

In contrast, shear-critical beam SH14 M exhibited typical shear behaviour with brittle diagonal fatal failure. First flexural cracks formed at mid-span and perpendicular to the longitudinal axis of the beam, whereas the increase of the applied load caused further flexural cracks to spread and inevitably initial diagonal cracks formed. Consequently, the formation of a critical shear crack on the left shear span of the beam caused its brittle failure. The plot of Fig. 8 presents the experimental behaviour of the beam in terms of shear load versus mid-span deflection curve. The cracking patterns of the beam at different levels of loading and corresponding damage are also displayed and compared in the photographs of Fig. 8.

It is mentioned that in the behavioural curves of Figs. 6 a and b, 7 and 8 each point "D" denotes a WiAMS measurement of all PZTs signatures that corresponds to specific displacement ductility and damage level.

Typical curves of the WiAMS measurements of the mounted PZT transducers to the tested RC elements are presented and compared in Figs. 9–11 . Especially, Fig. 9a and b display the voltage signal frequency response of "PZT2" and "PZT3" bonded on the steel bars of flexural beams FL10 M and FL12 M, respectively. Fig. 10 presents the signal plots of the PZT transducers mounted on the flexural element FL12C. "PZT1" and "PZT2" were bonded on the steel bars (internal PZTs) whereas "PZT X1" and "PZT X2" were externally bonded on the concrete surface of the RC element at positions very close to the internal PZTs (see also Fig. 2a). Fig. 11 shows the voltage signal frequency plots of the embedded transducers "PZT3" and "PZT4" inside concrete mass and the plots of the externally bonded patches "PZT X7" and "PZT X8" on the concrete surface of the RC shear-critical beam SH14 M

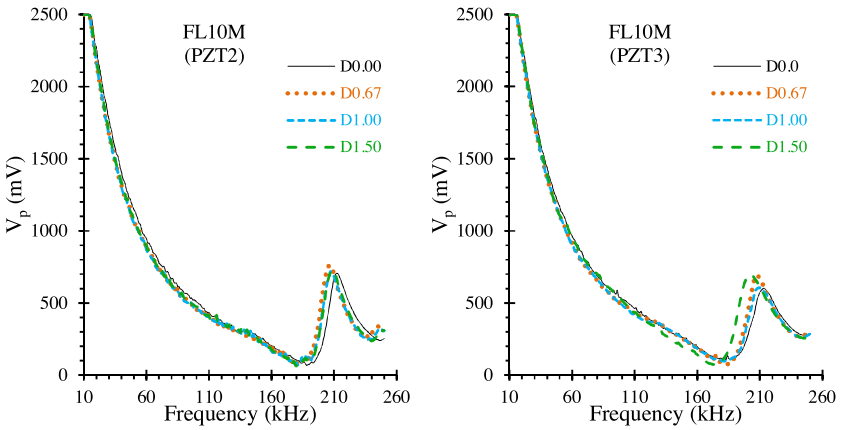

Fig. 9. Voltage signal frequency response of typical PZTs mounted on the steel bars of the flexural RC beams under monotonic loading.

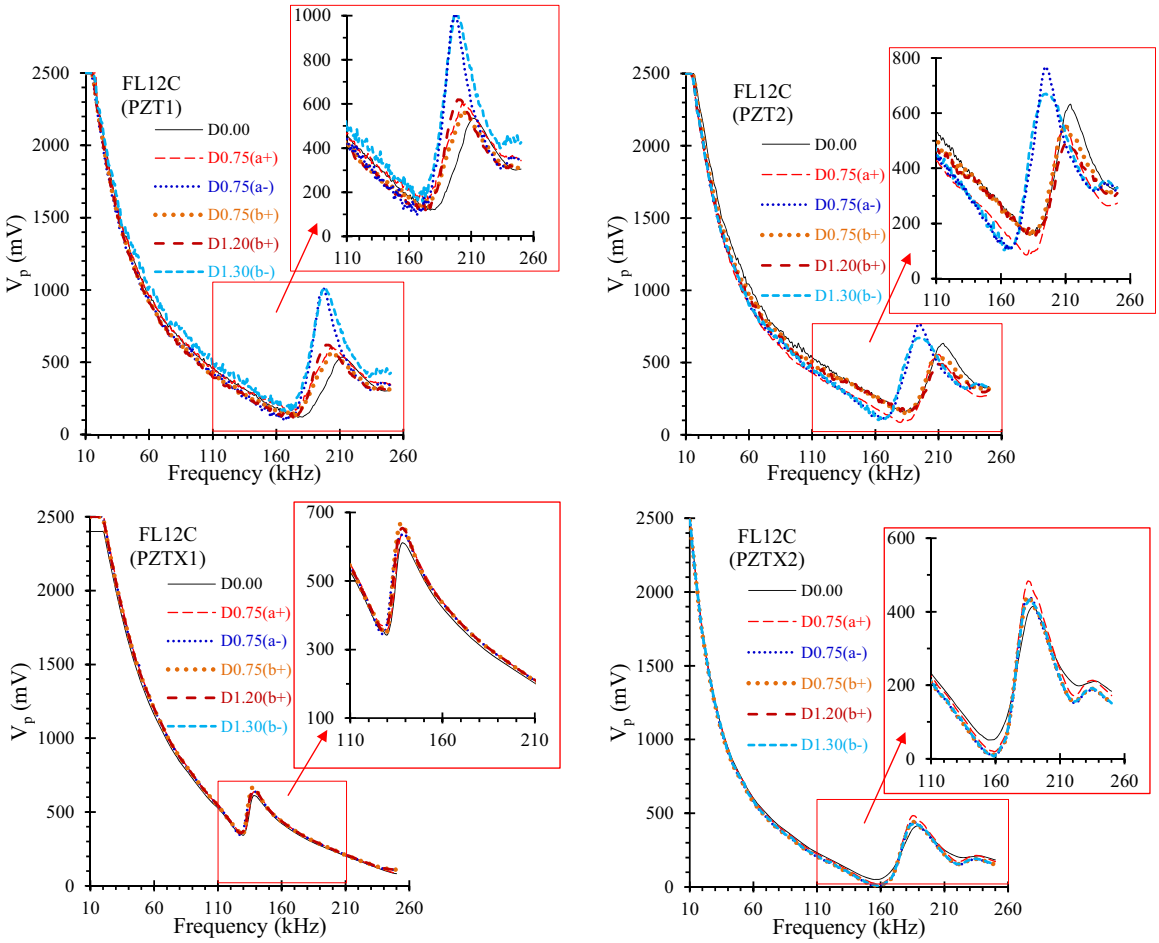

Fig. 10. Voltage signal frequency response of typical PZTs mounted on the flexural RC element under cyclic loading (FL12C).

(see also Fig. 2b for PZTs' positions reference). The frequency of the voltage signal response demonstrated in the diagrams of Figs. 9–11 ranges from 10 to 260 kHz. Close-ups of the frequency responses are also displayed in these Figs in order to discern the differences of the PZTs' signals between the healthy and the examined damage states.

The comparisons of the response curves in Fig. 9 indicate that there are certain discrepancies between the healthy and the damaged levels that have been measured from the bonded PZTs on the steel bars of both flexural RC beams FL10 M and FL12 M, especially in the frequency range 110–260 kHz. Similar discrepancies between the healthy and the damaged levels can also be observed from the signal measurements of the PZTs bonded on the steel bars of the flexural RC element FL12C in Fig. 10. It is noted that the signal plots of "PZT X1" and "PZT X2" externally bonded on the concrete surface of the RC element FL12C (Fig. 10) demonstrate less discrepancies than those of the bonded PZTs on the steel bars inside concrete although the external PZTs are very close to the internal ones. In addition, from the diagrams of Fig. 11 it is deduced that the discrepancies between the healthy and the damaged levels derived from the voltage signals of the embedded "smart aggregate" transducers "PZT3" and "PZT4" are clear and higher than the corresponding discrepancies of the externally bonded patches' signals "PZT X7" and "PZT X8" which seem to be rather slight. This indicates that externally bonded PZTs seem to be less sensitive than the embedded ones. However, it should be mentioned that the externally bonded PZT patches succeeded to measure voltage signals in more damage levels in the flexural element FL12C, whereas most of the bonded PZTs on the steel bars inside concrete mass failed to measure the voltage signals in the last damage levels. This is justified by the fact that yielding of the steel bars occurring at the last damage levels of the flexural element FL12C interrupted the operation of the bonded PZTs on these steel bars.

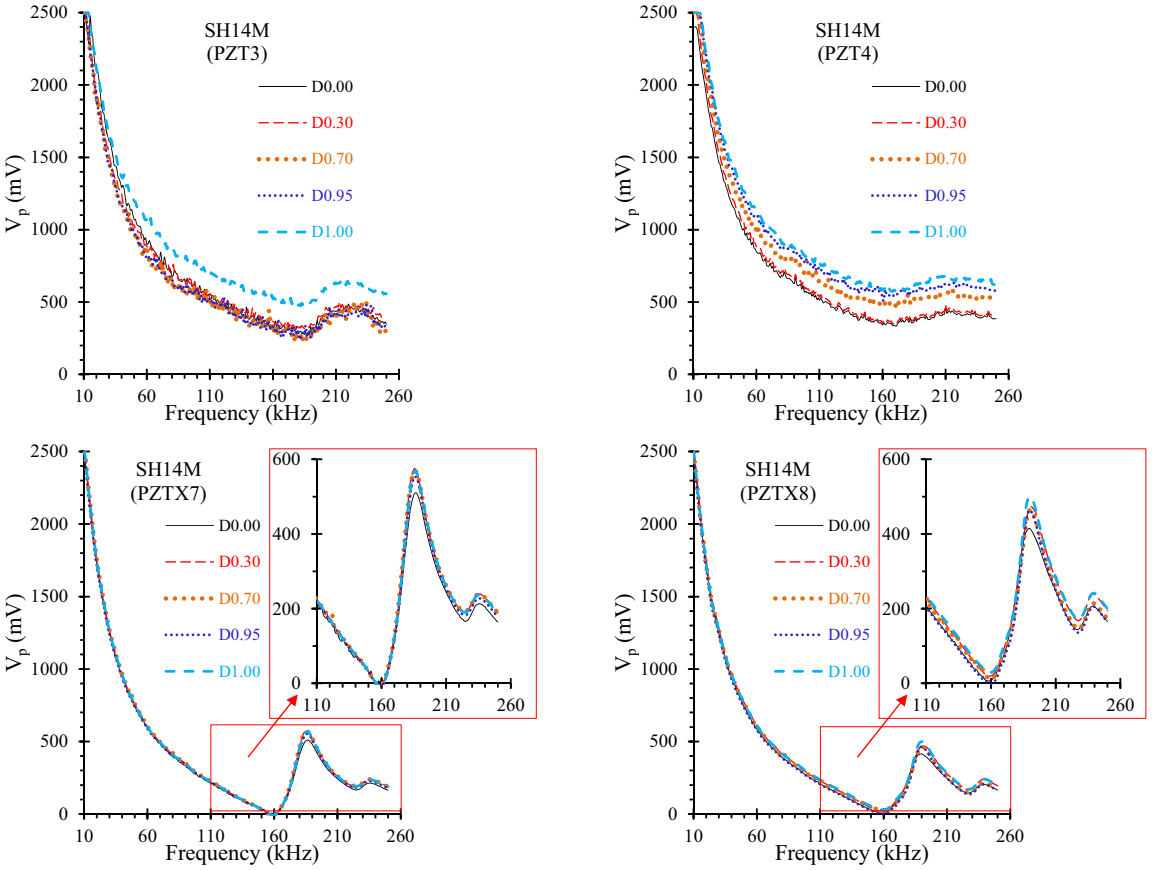

Fig. 11. Voltage signal frequency response of typical PZTs mounted on the shear-critical RC beam (SH14M).

3.5. Quantification of damage

The quantitative assessment of damage in concrete elements is traditionally made by the use of the statistically scalar damage values of Root Mean Square Deviation index (RMSD) [13]:

$$\mathrm{RMSD} = \sqrt{\frac{\sum_{1}^{N}\left(|V_p(\omega)|_D - |V_p(\omega)|_0\right)^2}{\sum_{1}^{N}\left(|V_p(\omega)|_0\right)^2}} \tag{8}$$

where: $|V_p(\omega)|_0$,$|V_p(\omega)|_D$ are the absolute values of the voltage signal measurements of the examined piezoelectric transducer at the baseline value (subscript 0) of the initial RC beam status ("Healthy" state) and at the examined damage level (subscript D) of the RC beam ("Damage 1", "Damage 2", etc.), respectively, and N is the number of measurements (the frequency index of each sum ranges from 10 kHz to 260 kHz).

Based on the adopted SHM technique principals, when damage occurred in any RC beam the voltage signal curves measured before damage (initial "Healthy" state) and after damage will change. The greater the damage, the greater the change in the voltage signal curves and, based on expression (8), the greater the absolute value of RMSD. Thus, the RMSD index can be used to evaluate the damage severity [2,47].

Figs. 12 a and b, 13 and 14 show the histogram of RMSD index values derived from the voltage signal measurements of the piezoelectric transducers mounted on the tested RC elements FL10 M, FL12 M, FL12C and SH14 M, respectively, for the examined damage levels at each RC element. In these Figs it is noticeable that for the majority of the PZTs, along with the increase of the damage level the values of RMSD calculated from their voltage signal measurements are trending upwards, confirming the increased damage severity. Moreover, PZTs that exhibit low or decreased RMSD values at high damage levels indicate low or negligible damage severity in the concrete region that they are located. Thus, comparisons of the RMSD values derived from an array of PZTs mounted at specific positions of the examined RC beam can locate the locus and the

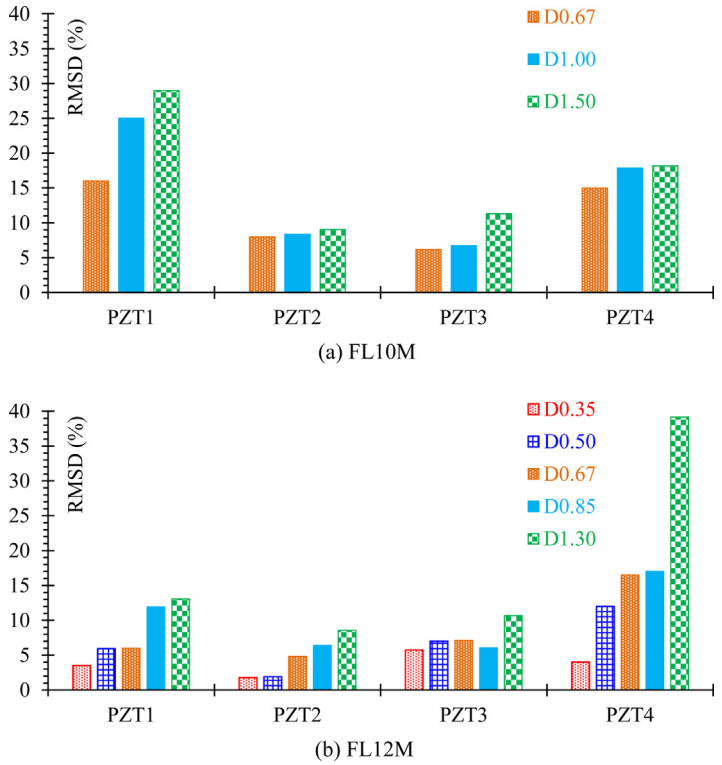

Fig. 12. RMSD index values of each PZT mounted on the flexural RC beams under monotonic loading.

magnitude of the occurred damage at different loading/damage levels. This is justified in detail by the following observations and remarks.

3.5.1. Flexural beam FL10 under monotonic loading

In Fig. 12a, the RMSD values of PZT1 that is installed on the left side of the mid-span of the steel bar of the beam (see also Fig. 2a) are the higher ones. This indicates that the severe flexural damage is located on the left side of the mid-span of the beam which is clearly verified from the cracking patterns of the beam in Fig. 6a.

3.5.2. Flexural beam FL12 under monotonic loading

In the same manner, in Fig. 12b, the RMSD values of PZT4 that is installed on the right side of the mid-span of the beam's steel bar (see also Fig. 2a) are the higher ones, revealing that the greater flexural damage is formed on the right side of the mid-span of the beam which is also verified from the cracking patterns of the beam in Fig. 6b.

3.5.3. Flexural element FL12C under cyclic loading

In Fig. 13 the RMSD values of PZT3 that is installed on the left side of the mid-span of the steel bar of the element (see also Fig. 2a) are slightly higher than the RMSD values of the other bonded PZTs. However, since flexural cracking and damage due

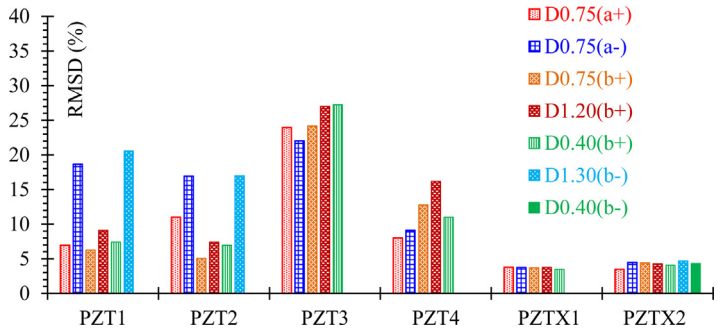

Fig. 13. RMSD index values of each PZT mounted on the flexural RC element under cyclic loading (FL12C).

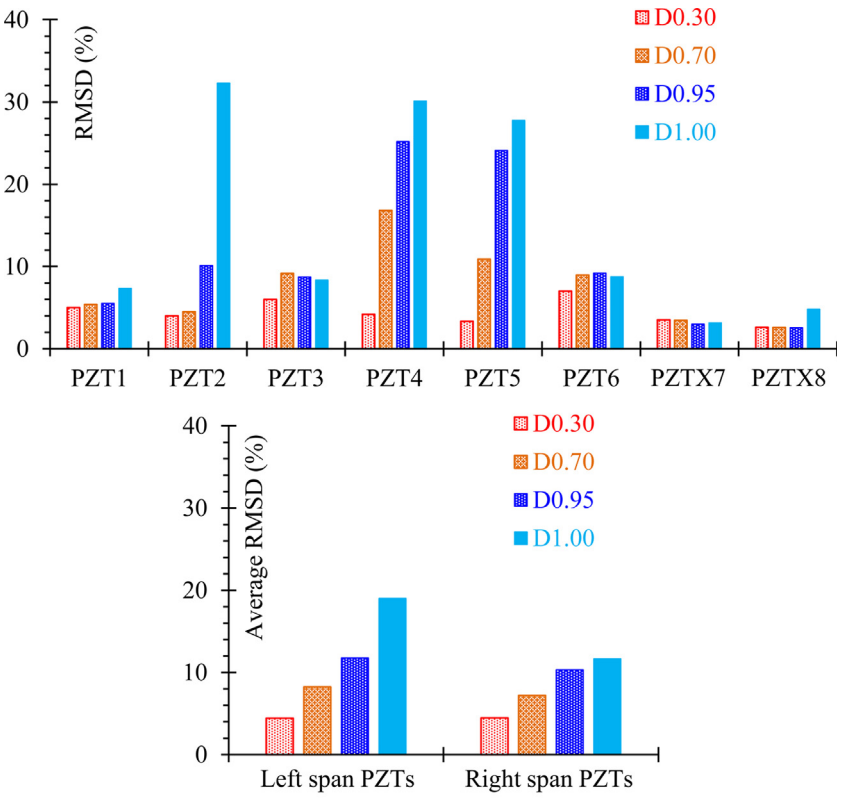

Photo 1: Cracking pattern at damage level "D0.95" (onset of shear diagonal cracking)

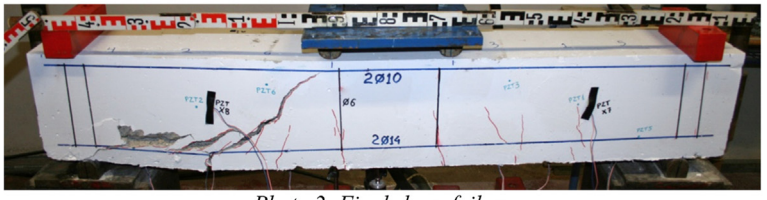

Photo 2: Final shear failure

Fig. 14. RMSD index values of each PZT mounted on the shear-critical RC beam (SH14M).

to cyclic deformations are spread on both sides of the mid-span of the element, as shown in Fig. 7, clear conclusions could not be deduced. Thus, although RMSD values in Fig. 12 show a general trend that indicates the suitability of the method to detect certain degrees of flexural damage under monotonic loading, the RMSD trends in Fig. 13 are not very strong. Nevertheless, RMSD values corresponded to the occurred damage level severity.

3.5.4. Shear-critical beam SH14 under monotonic loading

In Fig. 14 the RMSD values of the transducers PZT2, PZT4, PZT6 and PZT X8 mounted on the left shear span are higher than the RMSD values of the transducers PZT1, PZT5, PZT3 and PZT X7, respectively, which are mounted on the right shear span of the beam (see also Fig. 2b for PZTs' positions reference). This fact reveals that the eventual shear diagonal damage is located on the left shear span of the beam which is verified from the cracking patterns and the final failure mode of the beam, as shown in the photographs of Figs. 8 and 14. In addition, Fig. 14 also demonstrates and compares the average RMSD values of all four PZTs mounted on the left span with the average RMSD values of all four PZTs mounted on the right span of the shear-

critical beam SH14 M for the examined four loading/damage levels. In this diagram it is obvious that the average RMSD values of the PZTs mounted on the left span are higher than the corresponding values of the PZTs mounted on the right span, especially in the final damage level at failure (fourth damage level denoted as "D1.00"). This can clearly be confirmed from the experimentally obtained final failure mode shown in Fig. 8 and in Photo 2 of Fig. 14, since the fatal shear diagonal failure occurred in the left shear span. Nevertheless, the most important issue concerning the ability of the proposed SHM methodology to locate the locus and the magnitude of the occurred damage at different loading/damage levels is based on the following remarks:

- In the first damage level denoted as "D0.30" that corresponds to the first flexural crack (see also Fig. 8) the average RMSD value of the PZTs mounted on the left span is low and equal to the average RMSD value of the PZTs mounted on the right span since damage (slight flexural crack) occurred at the mid-span of the beam, far from both shear spans and far from the positions of the pre-installed PZTs.
- In the second damage level denoted as "D0.70" that corresponds to the propagation of the flexural cracking (see also Fig. 8) the average RMSD value of the PZTs mounted on the left span has increased compared to the previous damage level and it is slightly higher than the average RMSD value of the PZTs mounted on the right span. This is a minor indication concerning the prediction of the forthcoming formation of the diagonal cracking.
- In the third damage level denoted as "D0.95" that corresponds to the onset of the diagonal crack (see also Fig. 8 and Photo 1 of Fig. 14) the average RMSD value of the PZTs mounted on the left span has further increased compared to the previous damage levels and it is higher than the average RMSD value of the PZTs mounted on the right span. This leads to a safe determination of the location of the brittle shear failure at an early stage of damage (first slight diagonal crack shown in the Photo 1 of Fig. 14), ensuring that damage would inevitably occur on the left span, as actually happened and as can be verified from the cracking pattern of the shear-critical beam's final failure in Photo 2 of Fig. 14.

4. Conclusions

A new real-time integrated wireless SHM system named "WiAMS" is applied to detect and evaluate the damage severity level in flexural and shear-critical RC elements tested under monotonic and cyclic loading. It implements specially manufactured small-sized portable devices and the voltage signatures of an array of mounted smart piezoelectric transducers. Three different installations of PZTs have been examined; (a) epoxy bonded PZTs on the surface of the steel reinforcing bars of the flexural elements, (b) embedded PZTs inside the concrete mass of the shear-critical beam as "smart aggregates" and (c) externally epoxy bonded PZTs on the concrete surface of the tested elements. The positions of the piezoelectric transducers have been predefined before testing based on the anticipated flexural and shear diagonal cracking of the examined RC elements.

Voltage signatures of the PZTs acquired from the WiAMS measurements during tests demonstrated obvious discrepancies between the frequency response of the healthy and the examined damage levels for every RC element. These differences clearly indicate the presence of damage, whereas their gradual change in the nature of the frequency response reveals the magnitude of the occurred damage.

The statistical RMSD index has been used for the quantitative assessment of the damage. Test results proved that along with the increase of the damage level the values of RMSD calculated from the voltage signal measurements of the PZTs show a logical and consistent increase confirming the increase of the examined damage level. RMSD values of a mesh of PZT transducers arrayed in the RC elements provide satisfactory reliability for damage severity evaluation and lead to a safe determination of the locus and the magnitude of the occurred damage at different load levels.

Test results showed promising indications that the WiAMS measurements of a series of smart piezoelectric materials mounted on specific and predefined locations in RC constructions could help to diagnose damage and to predict forthcoming failures at early damage stages. Although the methodology shows potential for application in the field, further investigation is required before it has sufficient reliability for full implementation in existing structures, especially in earthquake prone regions. The influence of the developed stresses on the signals of the piezoelectric transducers, the baseline damage index values at specific RC elements and more tests, especially under cyclic reversal deformations should be examined and performed.

Acknowledgements

This research has been co-financed by the European Union (European Social Fund-ESF) and Greek National Funds through the Operational Programme "Education and Lifelong Learning" of the National Strategic Reference Framework (NSRF) – Research Funding Program: THALES. Investing in knowledge society through the European Social Fund. This study was also financially supported by the research project no. 81570 of the Special Account for Research Funds of Democritus University of Thrace.

References

[1] S. Bhalla, C.K. Soh, Electromechanical impedance modeling for adhesively bonded piezo-transducers, J. Intell. Mater. Syst. Struct. 15 (12) (2004) 955–972.
[2] S. Bhalla, A.P.R. Vittal, M. Veljkovic, Piezo-impedance transducers for residual fatigue life assessment of bolted steel joints, J. Struct. Health Monit. 11 (6) (2012) 733–750.
[3] C.E. Chalioris, M.J. Favvata, C.G. Karayannis, Reinforced concrete beam–column joints with crossed inclined bars under cyclic deformations, Earthquake Eng. Struct. Dyn. 37 (6) (2008) 881–897.
[4] C.E. Chalioris, Steel fibrous RC beams subjected to cyclic deformations under predominant shear, Eng. Struct. 49 (2013) 104–118.
[5] C.E. Chalioris, N.A. Papadopoulos, G.M. Angeli, C.G. Karayannis, C.P. Liolios AstA. Providakis, Damage evaluation in shear-critical reinforced concrete beam using piezoelectric transducers as smart aggregates, Open Eng. 5 (1) (2015) 373–384.
[6] C.E. Chalioris, C.P. Providakis, M.J. Favvata, N.A. Papadopoulos, G.M. Angeli, C.G. Karayannis, Experimental application of a wireless earthquake damage monitoring system (WiAMS) using PZT transducers in reinforced concrete beams, WIT Trans. Built Environ. 152 (2015) 233–243.
[7] A. Cladera, A.R. Marí, Shear strength in the new eurocode 2 a step forward? Struct. Concr. 8 (2) (2007) 57–66.
[8] A. Cladera, A. Marí, C. Ribas, J. Bairán, E. Oller, Predicting the shear-flexural strength of slender reinforced concrete T and I shaped beams, Eng. Struct. 101 (2015) 386–398.
[9] B.S. Divsholi, Y. Yang, Application of PZT sensors for detection of damage severity and location in concrete, Int. Soc. Opt. Eng. (2008) 726813.
[10] B.S. Divsholi, Y. Yang, L. Bing, Monitoring beam-column joint in concrete structures using piezo-impedance sensors, Adv. Mater. Res. 79-82 (2009) 59–62.
[11] B.S. Divsholi, Y. Yang, Combined embedded and surface-bonded piezoelectric transducers for monitoring of concrete structures, NDT&E Int. 65 (2014) 28–34.
[12] S. Hou, Y. Yu, H.B. Zhang, X.Q. Mao, J.P. Ou, A SA-Based wireless seismic stress monitoring system for concrete structures, Int. J. Distr. Sensor Netw. (2013) (Article ID 978313, 7 pages.).
[13] X. Hu, H. Zhu, D. Wang, A study of concrete slab damage detection based on the electromechanical impedance method, Sensors 14 (10) (2014) 19897–19909.
[14] C.G. Karayannis, C.E. Chalioris, Shear tests of reinforced concrete beams with continuous rectangular spiral reinforcement, Constr. Build. Mater. 46 (2013) 86–97.
[15] C.G. Karayannis, M.E. Voutetaki, C.E. Chalioris, C.P. Providakis, G.M. Angeli, Detection of flexural damage stages for RC beams using piezoelectric sensors (PZT), Smart Struct. Syst. 15 (4) (2015) 997–1018.
[16] C.G. Karayannis, C.E. Chalioris, G.M. Angeli, N.A. Papadopoulos, M.J. Favvata, C.P. Providakis, Experimental damage evaluation of reinforced concrete steel bars using piezoelectric sensors, Constr. Build. Mater. 105 (2016) 227–244.
[17] N. Kaur, S. Bhalla, Combined energy harvesting and structural health monitoring potential of embedded piezo-concrete vibration sensors, J. Energy Eng. ASCE 141 (4) (2015).
[18] C. Liang, F.P. Sun, C.A. Rogers, Coupled electromechanical analysis of adaptive material systems – Determination of the actuator power consumption and system energy transfer, J. Intell. Mater. Syst. Struct. 5 (1) (1994) 12–20.
[19] A.R. Marí, A. Cladera, J. Bairán, E. Oller, C. Ribas, Shear-flexural strength mechanical model for the design and assessment of reinforced concrete beams subjected to point or distributed loads, Front. Struct. Civil Eng. 8 (4) (2014) 337–353.
[20] J.-Y. Min, S. Park, C.-B. Yun, B.-H. Song, Development of a low-cost multifunctional wireless impedance sensor node, Smart Struct. Syst. 6 (5) (2010) 689–709.
[21] A.S.K. Naidu, C.K. Soh, Damage severity and propagation characterization with admittance signatures of piezo transducers, Smart Mater. Struct. 13 (2) (2004) 393–403.
[22] P. Negi, N. Kaur, S. Bhalla, T. Chakraborty, Experimental strain sensitivity investigations on embedded PZT patches in varying orientations, in: V. Matsagar (Ed.), Advances in Structural Engineering, Springer, India, 2015, pp. 2615–2620.
[23] K.-D. Nguyen, J.-T. Kim, Smart PZT-interface for wireless impedance-based prestress-loss monitoring in tendon-anchorage connection, Smart Struct. Syst. 9 (6) (2012) 489–504.
[24] C.P. Providakis, M.E. Voutetaki, Electromechanical admittance-based damage identification using Box-Behnken design of experiments, Struct. Durab. Health Monit. 3 (4) (2007) 211–227.
[25] C.P. Providakis, E.V. Liarakos, T-WiEYE: an early-age concrete strength development monitoring and miniaturized wireless impedance sensing system, Proc. Eng. 10 (2011) 484–489.
[26] C.P. Providakis, E.V. Liarakos, E. Kampianakis, Non-destructive wireless monitoring of early-age concrete strength gain using an innovative electromechanical impedance sensing system, Smart Mater. Res. (2013) (Article ID 932568, 10 pgs).
[27] C.P. Providakis, E.V. Liarakos, Web-based concrete strengthening monitoring using an innovative electromechanical impedance telemetric system and extreme values statistics, Struct. Contr. Health Monit. 21 (9) (2014) 1252–1268.
[28] C.P. Providakis, K.D. Stefanaki, M.E. Voutetaki, J. Tsompanakis, M.E. Stavroulaki, Damage detection in concrete structures using a simultaneously activated multi-mode PZT active sensing system: numerical modelling, Struct. Infrastr. Eng. 10 (11) (2014) 1451–1468.
[29] C.P. Providakis, G.M. Angeli, M.J. Favvata, N.A. Papadopoulos, C.E. Chalioris, C.G. Karayannis, Detection of concrete reinforcement damage using piezoelectric materials – analytical and experimental study, Int. J. Civil Arch. Struct. Constr. Eng. 8 (2) (2014) 197–205.
[30] C.P. Providakis, C.G. Karayannis, C.E. Chalioris, M.J. Favvata, G.M. Angeli, N.A. Papadopoulos, Usage of PZTs for damage evaluation of steel reinforcing bar, Sch. J. Eng. Technol. 3 (1B) (2015) 80–93.
[31] C. Ribas, A. Cladera, Experimental study on shear strength of beam-and-block floors, Eng. Struct. 57 (2013) 428–442.
[32] A. Savva, P. Manita, K.K. Sideris, Influence of elevated temperatures on the mechanical properties of blended cement concretes prepared with limestone and siliceous aggregates, Cem. Concr. Comp. 27 (2) (2005) 239–248.
[33] R. Shanker, S. Bhalla, A. Gupta, M.P. Kumar, Dual use of PZT patches as sensors in global dynamic and local electromechanical impedance techniques for structural health monitoring, J. Intell. Mater. Syst. Struct. 22 (16) (2011) 1841–1856.
[34] S.W. Shin, T.K. Oh, Application of electro-mechanical impedance sensing technique for online monitoring of strength development in concrete using smart PZT patches, Constr. Build. Mater. 23 (2) (2009) 1185–1188.
[35] K.K. Sideris, N.S. Anagnostopoulos, Durability of normal strength self-compacting concretes and their impact on service life of reinforced concrete structures, Constr. Build. Mater. 41 (2013) 491–497.
[36] C.K. Soh, K.K.-H. Tseng, S. Bhalla, A. Gupta, Performance of smart piezoceramic patches in health monitoring of a RC bridge, Smart Mater. Struct. 9 (4) (2000) 533–542.
[37] G. Song, H. Gu, Y.L. Mo, T.T.C. Hsu, H. Dhonde, Concrete structural health monitoring using embedded piezoceramic transducers, Smart Mater. Struct. 16 (2007) 959–968.
[38] G. Song, H. Gu, Y.L. Mo, Smart aggregates: multi-functional sensors for concrete structures – a tutorial and a review, Smart Mater. Struct. 17 (3) (2008) 033001.
[39] V. Talakokula, S.K. Dhawan, S. Srivastava, N. Kaur, S. Moharana, S. Bhalla, B. Bhattacharjee, A. Gupta, Recent advances in structural health monitoring based on EMI technique, International Conference on Trends and Challenges in Concrete Structures, Ghaziabad, UP, India, 2013 Paper No. 11501.
[40] V. Talakokula, S. Bhalla, A. Gupta, Corrosion assessment of reinforced concrete structures based on equivalent structural parameters using electro-mechanical impedance technique, J. Intell. Mater. Syst. Struct. 25 (4) (2014) 484–500.

[41] R. Tawie, H.K. Lee, Piezoelectric-based non-destructive monitoring of hydration of reinforced concrete as an indicator of bond development at the steel-concrete interface, Cem. Concr. Res. 40 (12) (2010) 1697–16703.
[42] A.-D.G. Tsonos, A new method for earthquake strengthening of old R/C structures without the use of conventional reinforcement, Struct. Eng. Mech. 52 (2) (2014) 391–403.
[43] M.E. Voutetaki, C.P. Providakis, C.E. Chalioris, FRP debonding prevention of strengthened concrete members under dynamic load using smart piezoelectric materials (PZT), Proceedings of the 15th European Conference on Composite Materials, ECCM 2012 – Composites at Venice, Venice, Italy, 2012, pp. 24–28.
[44] M.E. Voutetaki, N.A. Papadopoulos, G.M. Angeli, C.P. Providakis, Investigation of a new experimental method for damage assessment of RC beams failing in shear using piezoelectric transducers, Eng. Struct. 114 (2016) 226–240.
[45] D. Wang, H. Zhu, Monitoring of the strength gain of concrete using embedded PZT impedance transducer, Constr. Build. Mater. 25 (9) (2011) 3703–3708.
[46] D. Wang, H. Song, H. Zhu, Numerical and experimental studies on damage detection of a concrete beam based on PZT admittances and correlation coefficient, Constr. Build. Mater. 49 (2013) 564–574.
[47] D. Xu, X. Cheng, S. Huang, M. Jiang, Identifying technology for structural damage based on the impedance analysis of piezoelectric sensor, Constr. Build. Mater. 24 (12) (2010) 2522–2527.
[48] Y. Yang, A. Miao, Effect of external vibration on PZT impedance signature, Sensors 8 (11) (2008) 6846–6859.
[49] Y. Yang, Y. Hu, Y. Lu, Sensitivity of PZT impedance sensors for damage detection of concrete structures, Sensors 8 (1) (2008) 327–346.